Composites Part B 160 (2019) 546–557

Contents lists available at ScienceDirect

Composites Part B

journal homepage: www.elsevier.com/locate/compositesb

Experimental investigation of prepreg slit tape wrinkling during automated fiber placement process using StereoDIC

Sreehari Rajan, Michael A. Sutton*, Roudy Wehbe, Brian Tatting, Zafer Gürdal, Addis Kidane, Ramy Harik

McNair Aerospace Center and Department of Mechanical Engineering, University of South Carolina, Columbia, SC, 29208, United States

ARTICLE INFO

Keywords:
Prepreg tows
Automated fiber placement
Curvilinear steering
StereoDIC
Tow wrinkling and deformation measurements

ABSTRACT

For the first time, an experimental investigation is presented quantifying out-of-plane wrinkle formation and in-plane deformations occurring in prepreg slit tape specimens during automated fiber placement (AFP). The AFP process is conducted on 6.35 mm wide individual prepreg tows that are placed along a straight path and steered along circular paths with radii of curvature, $\rho = 2540$ mm, 1270 mm and 305 mm. Full-field shape, displacement and strain measurements are obtained using StereoDIC in three successive stages; (i) immediately after lay-up of the tow, (ii) one hour after lay-up and (iii) after reheating of the as-placed tow by traversing the AFP head close to the tow path and exposing the specimen to the same levels of heating as employed during the initial lay-up (without compaction pressure). Measurements obtained in stage (i) showed that (a) all tows exhibited local wrinkling at locations where the underlying substrate had defects (e.g., gaps, overlaps), (b) excluding the substrate defect locations, tows steered with $\rho = 2540$ mm showed no evidence of additional out-of-plane wrinkling after placement, (c) tows steered with $\rho = 1270$ mm exhibited several small amplitude wrinkles initiated at locations outside the substrate overlap regions and (d) tows steered with $\rho = 305$ mm incurred significant additional localized wrinkling along the inner radius of the tow with an increase in both the amplitude and frequency of the wrinkles. In addition, higher variability in the wrinkle wavelength is observed for $\rho = 305$ mm. Measurements obtained in stages (ii) and (iii) showed an increase in wrinkle amplitude, indicating that wrinkle amplitude is a function of both time and temperature for an as-placed tow.

1. Introduction

Due to their high strength to weight ratio and ability to be tailored to obtain desired properties in different directions, fiber-reinforced composite materials are increasingly being used in areas where weight reduction is a major consideration, especially in the aerospace industry [1]. However, manufacturing of complicated structures using composite materials has many challenges. The recent introduction of automated fiber placement (AFP) offers an efficient and accurate method for placement and bonding of prepreg tows along curvilinear paths to obtain variable stiffness properties that improve buckling performance and increase first ply failure strength [2]. The ability to steer tows at preferred orientation opens a wide range of design options for tailoring properties in composite laminates. It has been shown by Gürdal et al. [3,4] that orienting fibers within each lamina along optimal paths can result in favorable stress distributions and improved performance of a laminate for specific applications. Buckling analysis of variable angle tow composites performed by Cheng et al. [5] and Wu et al. [6] has shown that buckling resistance can be significantly improved by optimizing the tow placement path.

To perform adaptive tow placement, modern AFP systems are equipped with a computer controlled robotic arm to lay-up bands of tows (8–32 bands) along predefined paths [7]. During the AFP process, tows are heated via an infrared light source[1] and adhered to a substrate by using a compaction roller that applies pressure to the tow during placement. Application of the compaction pressure improves adherence of the heated tows by removing voids that tend to form in the laminate during lay-up. Depending on the properties of the tow (prepreg tack, elastic moduli of materials) and process parameters (contact pressure, temperature, lay-up speed), there is potential to introduce defects during manufacturing that compromises the strength and fatigue life of the laminate. As noted in Ref. [8], there are a variety of deformation mechanisms (intra-ply shear, tension and ply bending) that occur during processing of continuous, aligned fiber systems, and these

* Corresponding author.
E-mail address: sutton@sc.edu (M.A. Sutton).

[1] Other methods used for tow heating during AFP include hot gases and high-power laser illumination.

https://doi.org/10.1016/j.compositesb.2018.12.017
Received 28 July 2018; Received in revised form 16 November 2018; Accepted 3 December 2018
Available online 05 December 2018
1359-8368/ © 2018 Published by Elsevier Ltd.

deformations will affect the quality of the resulting composite system. For example, tows placed along curvilinear paths have an inherent mismatch in length along the inner and outer radii, resulting in a natural tendency for the tow to separate and develop out-of-plane wrinkles along the inner radius.

In addition to out-of-plane wrinkling due to length mismatch across a tow, other common types of defects found in the steered tows [9] are (a) localized delamination from the substrate, (b) splitting of tows due to in-plane shear and (c) in-plane buckling. Identifying the ideal combination of heating and local pressure to be applied during AFP of tows steered along curvilinear paths is essential to increase adhesive strength and maximize the quality of the as-placed tows so that the manufactured component will have optimal strength and fatigue life. Defining the "critical tow path" as that curvilinear path along which a tow can be steered without incurring measurable localized out of plane wrinkling or related defects, it is important that the minimum steering radius (ρ_c) for the critical tow path [10] be determined.

Various measurement and modeling techniques have been developed in recent years in an attempt to identify the optimum process parameters and quantify the critical ρ_c so that the number of defects in the AFP steered laminates can be minimized. To measure in-situ temperature and strain during the AFP process, Ebrahim et al. [11] used two fiber Bragg grating (FBG) sensors between the 2nd and 3rd plies that are placed at 15° angles relative to each other. Each FBG could also act as a structural health monitoring system (SHM) to detect the effect of flaws, while providing strain and temperature measurements. The authors also showed that acoustic emission could detect the onset of local flaw growth. The authors obtained temperature and strain data for a CF/PEEK composite (10 plies) during placement of the 4th to 10th plies. However, validation of the accuracy of measurements has yet to be completed, an essential aspect of such experiments since placement of the FBG sensors can have an adverse effect on the adhesion of a tow to the substrate.

In addition to the experimental work noted above, there has been considerable modeling effort directed towards prediction of the critical radius of curvature. For example, Matveev et al. [12] formulated a closed form solution to model wrinkle formation in steered tows with different radii of curvature, ρ. Their analytical expression is based on elastic buckling of an orthotropic plate on an elastic foundation. An approximate solution to their model for wrinkle formation was obtained by using the Raleigh-Ritz method. The authors also obtained an expression for ρ_c. Beakou et al. [13] published similar work in which the authors developed an approximate solution for the response of an orthotropic plate on an elastic foundation to determine the critical buckling load and minimum steering radius when there are simply supported boundary conditions on three edges and a free boundary on the edge where wrinkling occurs. The authors also performed sensitivity analysis to show that the most important factors affecting critical buckling load are prepreg tack and tow width. It is noted that (a) the effect of delamination and viscoelasticity are not considered in either of these analytical models, (b) neither model is able to predict in-plane wrinkling or other defects and (c) neither the assumed in-plane load distributions nor the assumed out-of-plane wrinkle shape has been validated experimentally.

Several finite element (FE) based models have also been developed for determining conditions during thermo-forming operations that result in defect formation [14–17]. Recently Bakhshi et al. [18] used finite element modeling of the AFP process to predict various defects observed during layup of a 6.35 mm wide tow on an aluminum substrate. In their work, the tow was modelled as an elastic shell and cohesive zone modeling was used represent the adhesion of tow with the substrate. Comparison of their model prediction with photograph of the actual tow surface shows that the model was able to predict out of plane wrinkling and localized delamination of the tow (blister). However, neither the amplitude nor wavelength of the wrinkles were correlated with the FE results. Comparisons of these FE model predictions to experimental observations are typically performed through qualitative comparison of model predictions to photographs of the wrinkle shape/defects without direct comparison of quantitative metrics which is an indispensable part of FE model validation. The in-situ measurement of tow response during AFP processing has yet to be demonstrated and is the focus of the enclosed work.

Regarding experimental characterization, recent work has been performed [19] by the authors using the StereoDIC non-contacting measurement method to quantify the full-field deformations and wrinkles that occur for thermoplastic tows that are steered along curvilinear paths, but *not adhered to the substrate*. Results from this study show that (a) uplift (wrinkling) occurs on the compressive side of the tow for circular paths with radii of curvature, ρ, in the range 305 mm ≤ ρ ≤ 2540 mm, (b) the tensile side remains nominally flat on the surface of the planar substrate and (c) the wrinkle mode shape is the same for most specimen widths and various ρ. The lone exception is the narrowest tow width (9.5 mm) and the smallest ρ = 305 mm, where the uplifted shape flattens near the centerline as the tape rotates out of plane by 90^0 and more, (d) the amplitude of wrinkling increases with increases in ρ in all but the exceptional case noted above and (e) increasing the temperature of the prepreg tape from 25 °C to 110 °C does not alter the wrinkle shape, whereas increasing the temperature above the glass transition temperature and within the range $150^{u}C \rightarrow 350$ °C results in reduced amplitude and localized kinking of the specimen near midspan. With the exception of these recent studies, experimental data for wrinkle shape, wrinkle spacing and full-field deformations in tows that are placed and adhered to the substrate along curvilinear paths does not exist.

Taking advantage of the developments presented in Ref. [19], the enclosed work focuses on experimental characterization of the shape and deformation of AFP processed tows that are adhered to the substrate. StereoDIC [20–24], also known as 3D-DIC, is employed to obtain full-field, three-dimensional surface displacement data on the tow during AFP processing to improve our understanding of the mechanisms associated with wrinkling and other forms of defects. To this end, an experimental setup is developed using StereoDIC to investigate wrinkling modes and measure both the shape and deformation of as-placed and adhered tows as a function of towpath steering radius of curvature. In-contrast to conventional point-based measurements, StereoDIC provides full-field displacement and strain data which is advantageous when performing model validation and Finite Element Model Updating [25]. The paper is divided into four sections. Section 1 provides a brief introduction, including some of the recently completed background work. Section 2 describes the experimental process, including details regarding the AFP and the experimental StereoDIC setup employed to obtain deformation and shape measurements during processing. Sections 3, 4 and 5 present the Experimental Results, Discussion of Results and Summary of the findings, respectively. Section 6 acknowledges those contributing to the completion of the work and Section 7 provides a list of references.

2. Experimental setup and procedures

2.1. Stereovision measurement system

A typical StereoDIC setup consists of a stereo camera pair, mounting frame for the stereo cameras, tripod to mount the cameras and frame, a calibration grid for the cameras, a dedicated computer with digital image correlation software installed (VIC-3D) [26] and a suitable high contrast speckle pattern on the surface of the tow. Since many of the details regarding the stereovision system used in this study are similar to those described in Ref. [19], a brief summary of the key camera and lens parameters used in this work is given in Table 1. As noted in Ref. [19], linear polarizing filters for both the LED light and the camera

Table 1
Camera and lens parameters for stereovision system.

	Camera and lens parameters
Camera	5 MP CMOS PointGrey camera, 2448 × 2048 pixels^2 array 3.45 μm pixel size
Calibration	12 × 9 dot grid, 1.5 mm dot size, 5 mm dot spacing More than 120 stereo image pairs
Lens	Nikon Micro-Nikkor 25 mm focal length
Lens Filter	Linear polarizer
Light Source	LED with linear polarizing film
Lens Distortion	3rd Order Radial Distortion Correction

Table 2
StereoDIC parameters.

	StereoDIC parameters
Subset size	25 × 25 pixels^2
Step size	7 pixels
Filter type	Center-weighted Gaussian filter
Strain Filter size	5 × 5 data points (area of 35 × 35 pixels^2)
Strain measure	Lagrangian large strain tensor definition for all strain components
Field of view	114 mm × 95 mm
Magnification	0.045 mm/pixel
Average speckle size	0.15 mm

lenses are required for these studies since it is not possible to coat the specimen surface and remove reflections[2]; additional coatings applied to the tow (e.g. paint) altered the mechanical response of the flexible tow. The linear polarizers are adjusted to remove strong reflections from the images and provide a high contrast pattern with minimal reflectivity. Next, to obtain a white speckle pattern that could withstand the wear and elevated temperature conditions associated with the AFP process, two pattern application methods are evaluated. First, a fine spray of high temperature white flat paint (stable up to a maximum of 700 °C) is applied to form a speckle pattern on the tow surface. The natural black background on the tow surface with the white dots of spray paint gave good contrast pattern on the tow surface. In the second approach, white airbrush paint is applied with an airbrush system to create a speckle pattern. Both types of speckle pattern are evaluated for resistance to abrasion due to friction between the compaction roller and other contact areas in the tow feed and guidance system inside the AFP head. Both the high temperature paint and the airbrush paint are observed to give similar abrasion and temperature resistance at the maximum temperature that occurs during the automated fiber placement process. Thus, both methods could be used effectively.[3] Since the authors found better control of the speckle pattern size using the airbrush process, all speckle patterns used in this work are applied using an airbrush. By varying the size of the airbrush needle, the average speckle size is adjustable for a given application. The StereoDIC parameters[4] selected for this work are shown in Table 2. Finally, the calibration process followed the general procedure outlined in Ref. [19], though the calibration target used in these studies had different physical dimensions. The calibration target dot size and spacing are given in Table 1.

2.2. Data stitching for AFP experiments

To characterize the full-field behavior of a 6.35 mm wide by 610 mm long tow undergoing AFP processing, it is necessary to use relatively high magnification imaging to obtain accurate deformations across the width of the tow with available digital cameras.[5] To obtain the required spatial resolution over the complete length and width of the tow, one of two methods is used; (a) Multiview stereo system incorporating several stereo camera pairs to capture the complete length of the tow or (b) Single stereo camera system used to capture images by rigidly translating and rotating the system to acquire images spanning the entire tow length. For the second method using a single stereo camera pair, the tow remains stationary during the image acquisition process for both the reference (pre-AFP) and deformed (post-AFP) configurations. This is an important requirement for the single camera stereo system, as there is a time lapse between each successive image pair from one end to the other end as the stereo camera pair is translated along the tow length. If the pre-AFP and post-AFP tow lengths continue to move and are not stationary, the first method (Multiview stereo system) should be used. In this work, it is observed that the tow remained stationary in the reference and deformed configurations for the duration of the image acquisition (30 s). Hence the second method (b) is implemented in this work.[6]

As discussed in a recent book by one of the authors [27] and demonstrated conclusively in the first known experiment on a commercial jet-liner in 1995 [28], once a stereovision system is calibrated, then the stereo camera pair can be moved as a unit without affecting the calibration or measurement accuracy. For this to be true, the relative position of the two cameras in the stereo vision system should be fixed and the internal parameters in both cameras (e.g., focal lengths, distortion correction parameters) should remain the same. To meet these requirements, cameras typically are mounted on a rigid platform to ensure that no relative motion occurs between the two cameras.[7] A schematic of the image acquisition method implemented in this work is shown in Fig. 1. The stereo images are numbered 1 to N, with 1 on the left end and N for the right end of the tow. All the neighboring images are configured to have an overlap of ~15–20% of the field of view (FOV). The speckle images of the overlap region are used to obtain the rigid body coordinate transformation matrix between the two stereo camera systems and align neighboring image coordinates. Since the only difference between positions in the overlapped region obtained by the stereovision system before and after repositioning is a general rigid body motion, this observation can be used to "stitch together" common regions and extract shape and deformation data from different portions of the tow in a common coordinate system with relatively high spatial resolution. The process outlined above is used to obtain overlapping images for both the reference and deformed configurations of the tow. It is noted that the authors placed markers on the tow surface to assist in identifying the matching image sets in the reference and deformed

[2] Any specular reflection from the measured surface will be detrimental to the correlation of speckle images [27].

[3] In this study, the maximum temperature of the tow during placement is in the range of 40–50 °C and airbrush paint wis found be stable in this range, for AFP/ATL process involving higher temperatures the high temperature resistant paint may be required [19].

[4] An estimate for the accuracy of the strain measurements using StereoDIC is obtained by performing image correlation of multiple speckle images taken in the reference configuration. Results confirm that the standard deviation in the strain measurements for the parameters noted above is ~150 με.

[5] The field of view is much smaller than the physical length of the tow to obtain the required measurement spatial resolution with available 5 MP digital cameras. Thus, multiple high magnification images are obtained along the length of the tow and used to extract deformation data spanning the entire tow width and length.

[6] A Multiview camera system could be used in this work. However, it is more expensive, requiring several cameras and more sophisticated image acquisition. Furthermore, a typical multiple camera system is arranged along a straight line in the reference position, making it less flexible when imaging steered tows having a range of radii of curvature.

[7] In order to check whether the cameras remain calibrated, the authors repeated the calibration process after each movement of the stereo system and compared the calibration parameters obtained before and after system movement. Results indicated negligible difference between the parameters for our studies, confirming that initial calibration parameters could be used to extract reliable measurements.

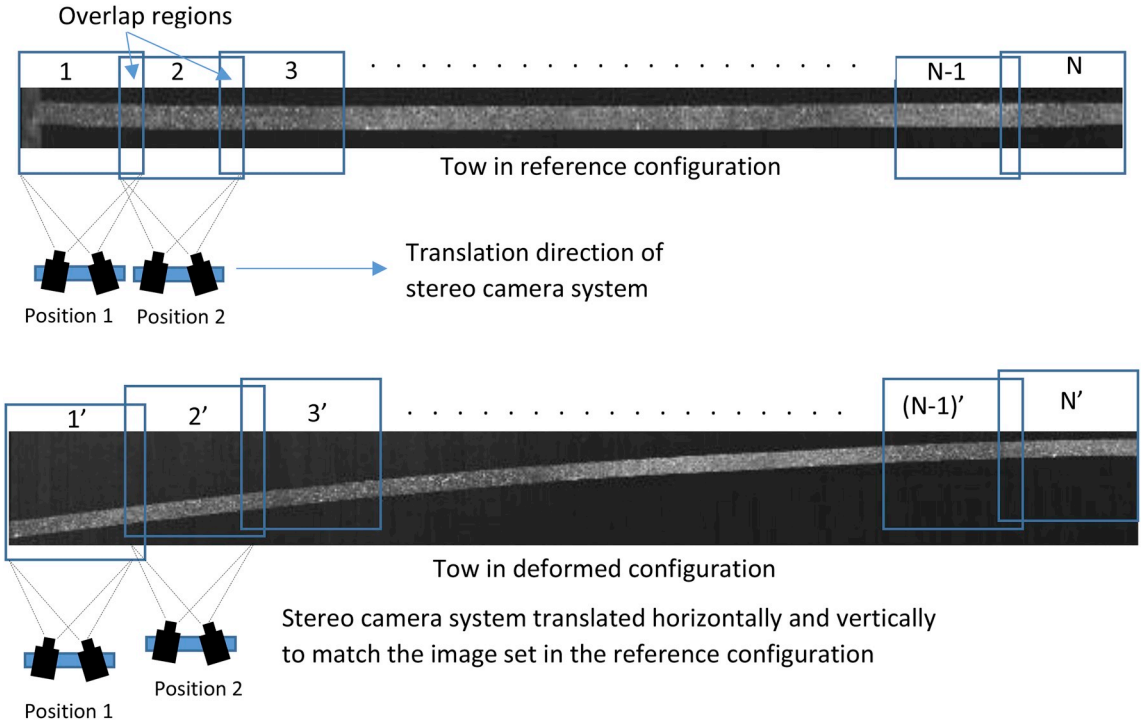

Fig. 1. Schematic of the image acquisition process.

positions.[8]

The process outlined in the previous paragraph provides a direct way to obtain the required full-field displacement and strain data along the entire tow length. Straightforward analysis of the imaging process in our studies confirmed that the maximum length of tow that can be imaged while ensuring adequate spatial resolution across the width of the tow is ~114 mm. To obtain deformations along the entire length of the tow, the camera pair is moved as a rigid body approximately 90 mm a total of 8 times and images are acquired of adjacent regions with ~20% overlap. Post-processing using a stitching process to relate rotated and translated stereo camera coordinate systems is performed using a built in Multiview option in VIC-3D [26] to combine all the full field data along the entire length of the tow into a global coordinate system. The general procedure for data stitching is as follows.

- Correlate the speckle images in the matching images sets of reference and deformed coordinate system (for example image set 1 and 1′ shown in Fig. 1) to obtain displacement and strain data in the reference image set coordinate system.
- Using the translation vector between the coordinate system and transformation matrix obtained from the overlap region, transform the displacement and strain data from all the image sets to the first image set coordinate system. For the 3rd to N^{th} image sets this involves multiple operations of transformation ($A_{N1} = [A_{21}].[A_{32}]$ …. $[A_{N(N-1)}]$ where A_{ij} is the transformation operation from j^{th} image set coordinate system to i^{th} image set coordinate system).

2.3. AFP lay-up process and stereovision imaging

The prepreg slit tape used for AFP lay-up is a 6.35 mm wide Hexcel IM7G/8552-1 unidirectional prepreg slit tape. A commercial AFP system (Horizontal Lynx® AFP from Ingersoll Machine Tools) in the McNair Aerospace Center at the University of South Carolina is used to perform the fiber placement of tows along predefined paths using an offline program. Four different fiber paths are programmed for lay-up of tows including a straight path and three circular paths with $\rho = 2540$ mm, 1270 mm and 305 mm. All process variables including lay-up speed (2438 mm/min), temperature (40 °C) and compaction force (200 N) are maintained throughout the layup process. All the tows are placed on a substrate laminate of the same material [90/0/90].

To apply the speckle pattern and capture reference speckle images (un-deformed configuration), tows are manually drawn from the machine head and straightened with light tension on a flat plate using masking tape (see Fig. 2). After applying the speckle pattern to the whole length of the tow, slightly overlapping images with FOV of 114 mm × 90 mm spanning the length of the tow are obtained in the reference configuration. Once the entire length of the tow has been speckled and imaged, the tow is rewound onto the spool in preparation for AFP processing. For each tow path, speckle images spanning the entire length of the tow, with up to 20% overlap between the images, are captured just after the tow is placed on the substrate; the time required to obtain these images is less than 30 s. For investigating the influence of time and the effect of heating during the placement of neighboring tows on the already placed tow, the process is repeated to capture additional set of images (a) one hour after placement and (b) re-heating of the as-placed tow by exposing the specimen to the same levels of heating as employed during the initial lay-up without mechanical loading.[9] Heating is performed using the IR heating element of the AFP system, which is brought very close to the steered tow (within 38 mm) as it is traversed along the length of the tow at 2438 mm/min.

Fig. 3 shows images of the four tows after undergoing AFP along a straight path and along circular arcs with $\rho = 2540$ mm, 1270 mm and 305 mm. To combine the data obtained from multiple images for each tow path and experimental condition, the stepwise shifting procedure outlined in Section 2.2 is performed. Each set of deformed images is compared with the reference (un-deformed) image set to obtain the

[8] The white markers added to the tow to assist in identifying corresponding images in the reference and deformed configuration of the tow are larger than a physical camera pixel size and spaced at an interval of 90 mm.

[9] Reheating is performed immediately after measurement in (a) and DIC measurement on the reheated tow is completed within 30 s.

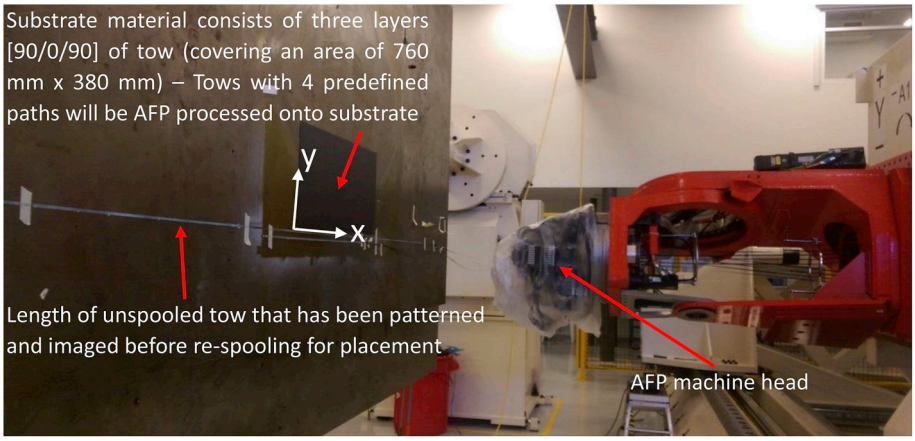

Fig. 2. Photograph of the tool, initial layers of [90/0/90] composite substrate, AFP head and initial length of patterned, unspooled tow that is imaged before re-spooling.

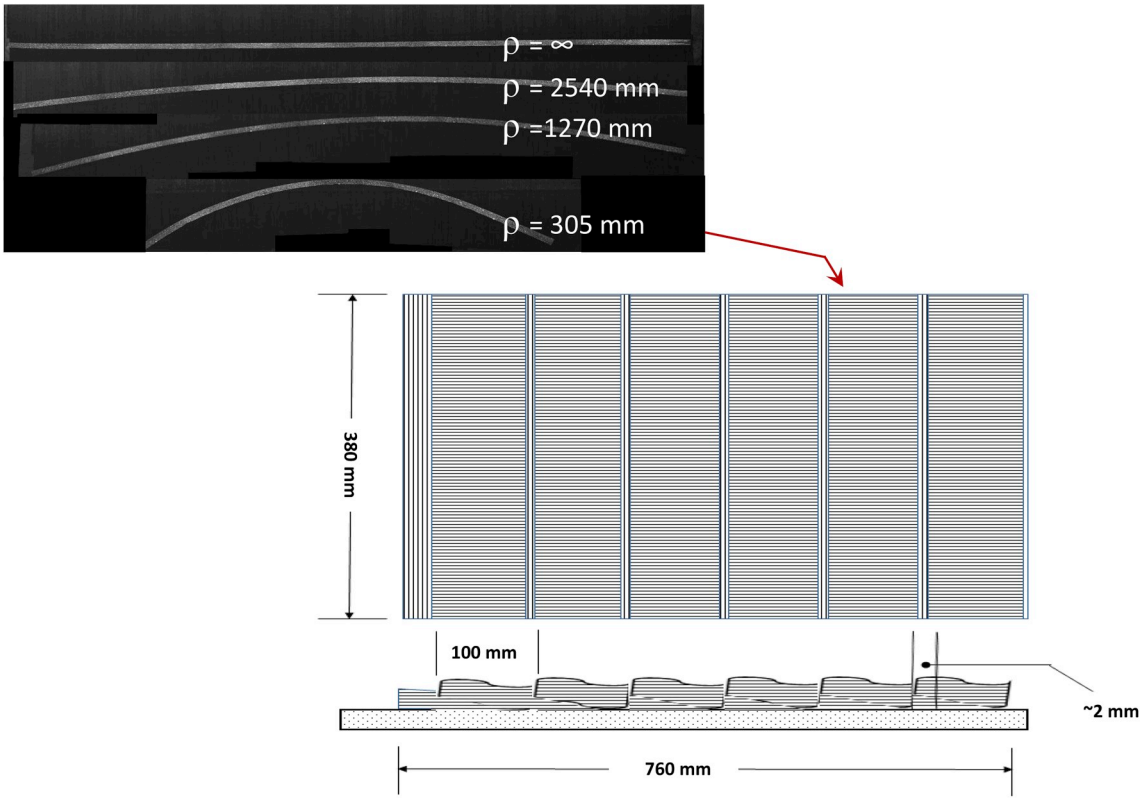

Fig. 3. Speckle images of four different tow paths. The top path is straight. The second and third paths from the top have ρ = 2540 mm and ρ = 1270 mm, respectively. The fourth or bottom path has ρ = 305 mm. INSET: Geometry of as-fabricated composite substrate for AFP of tows. Overlap of the substrate tows occurs every 100 mm in horizontal direction, resulting in periodic "defects" in tow substrate.

shape and out-of-plane deformations of the tow. For all experimental results reported in the remainder of the article, analysis of the speckle images is performed using commercial DIC software, VIC-3D [26], with the StereoDIC parameters shown in Table 2.

3. Experimental results

3.1. Out-of-plane wrinkle shape after AFP lay-up along a straight path

The deformed shape of the entire tow length along the straight path defined in Fig. 3 is shown in Fig. 4. As shown in Fig. 4, there is a clearly visible, regular, repeating pattern of out-of-plane wrinkling located every ~100 mm along the length. Further investigation of this surface profile confirms that these local variations in the shape of the straight tow are due to the presence of gaps and overlaps in the as-manufactured laminate substrate[10] shown in Fig. 3. Thus, the observed local out-of-plane wrinkle for the straight tow shown in Figs. 4–6 reflect the structure of the substrate and are not indicative of wrinkling due solely to deformation of the tow during placement.

[10] The laminate substrate is fabricated by placing sixteen, 6.35 mm tows side-by-side in one pass using the AFP system and then repeating this process by moving the AFP head in a raster pattern.

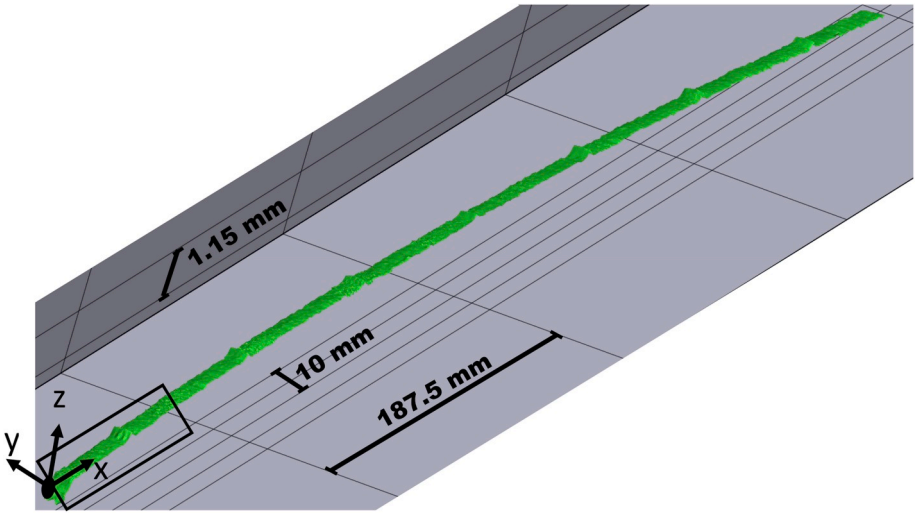

Fig. 4. Shape of the tow after placement along a straight path.

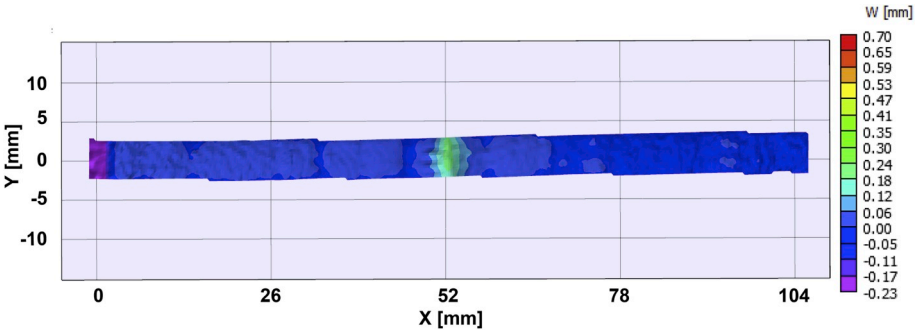

Fig. 5. Out-of-plane deformation map of the straight tow in the region highlighted by rectangular box in Fig. 4.

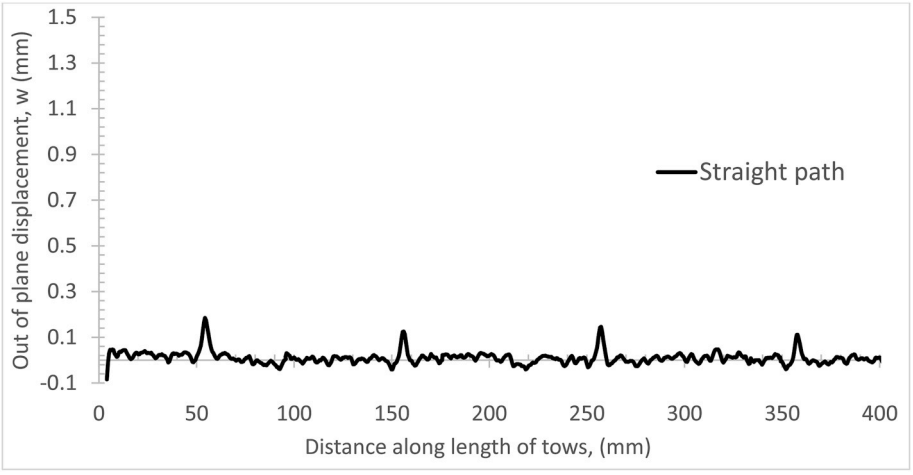

Fig. 6. Out-of-plane deformation along length of a straight tow. Plot corresponds to displacements along a line 1 mm above the bottom edge).

3.2. Out-of-plane wrinkle shape after AFP lay-up along three curved paths

Figures 7-8, 9-10 and 11-12 show the shape of the tows steered along circular paths with $\rho = 2540$ mm, 1270 mm and 305 mm, respectively.[11] Comparison of the out of plane displacements along the length of tows for $\rho = \infty$, 2540 mm, 1270 mm and 305 mm are shown in Fig. 13. As shown in Fig. 13, all four tows experienced local wrinkling at the four locations where laminate substrate defects are present. Thus, the relatively small laminate substrate imperfections, on the order of the tow thickness of 0.100 mm, act as nucleation cites for local wrinkling in all cases.

For $\rho = 2540$ mm and 1270 mm, inspection of Figs. 7, 9 and 13 shows that, to a reasonable approximation, other than the wrinkles due to imperfections in the substrate, there are no large wrinkles in the tow after placement for either case. However, additional inspection of Fig. 13 for $\rho = 1270$ mm indicates that there are several small amplitude local wrinkle initiation sites (wrinkle height $<$ 0.080 mm). Since

[11] The imperfections due to the overlapping tows in the substrate are also present in each of these cases.

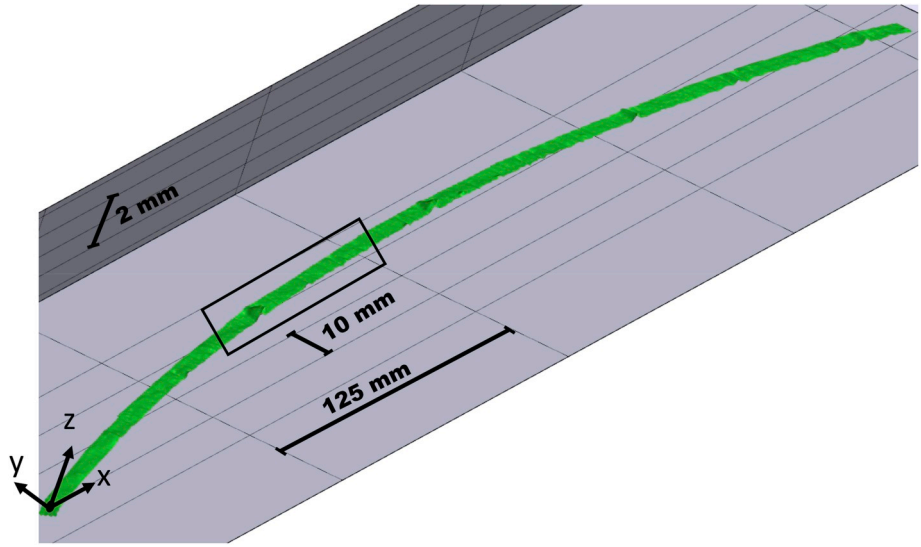

Fig. 7. Shape of the tow after placement along a circular path with ρ = 2540 mm.

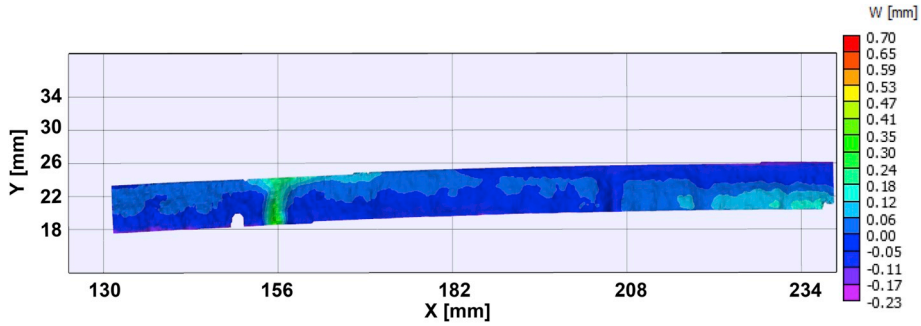

Fig. 8. Out-of-plane deformation map of the tow in the region highlighted by rectangular box in Fig. 7 for ρ = 2540 mm.

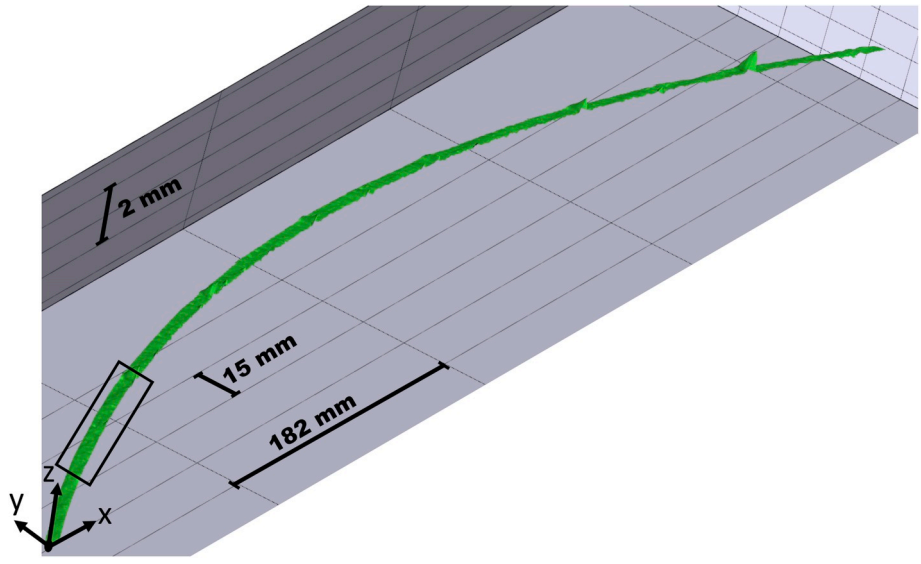

Fig. 9. Shape of the tow after placement along a circular path with ρ = 1270 mm.

the amplitude is much larger than the StereoDIC measurement variability for w(x,y,z) of 0.006 mm, these smaller, separate wrinkles are not entirely noise in the data but appear to be due to a combination of substrate surface variations and initiation of tow wrinkling due to local conditions including tow deformation.

For the smallest radius of curvature, ρ = 305 mm, there is a remarkable difference in the wrinkle amplitude and frequency. Here, the number and amplitude of new local wrinkles that are not due to substrate defects have increased significantly. Magnified views of the interaction of the local substrate imperfections and the deformation of the tow for ρ = 305 mm are shown in Figs. 12 and 14. Defining the measured distance between the peaks of adjacent wrinkles as the

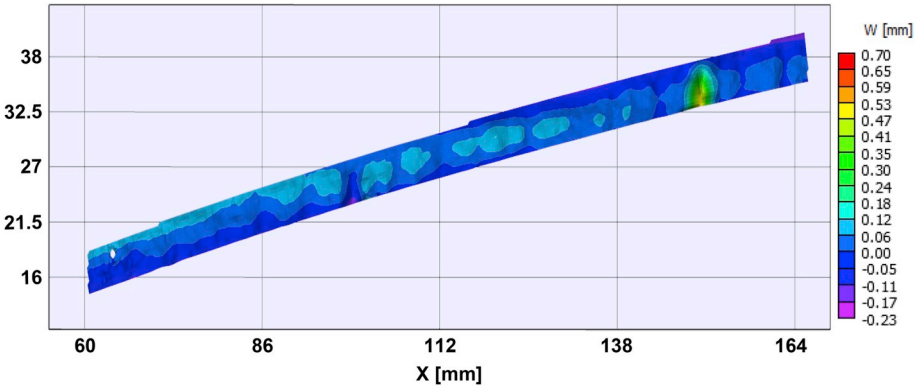

Fig. 10. Out-of-plane deformation map of the tow in the region highlighted by rectangular box in Fig. 9 for ρ = 1270 mm.

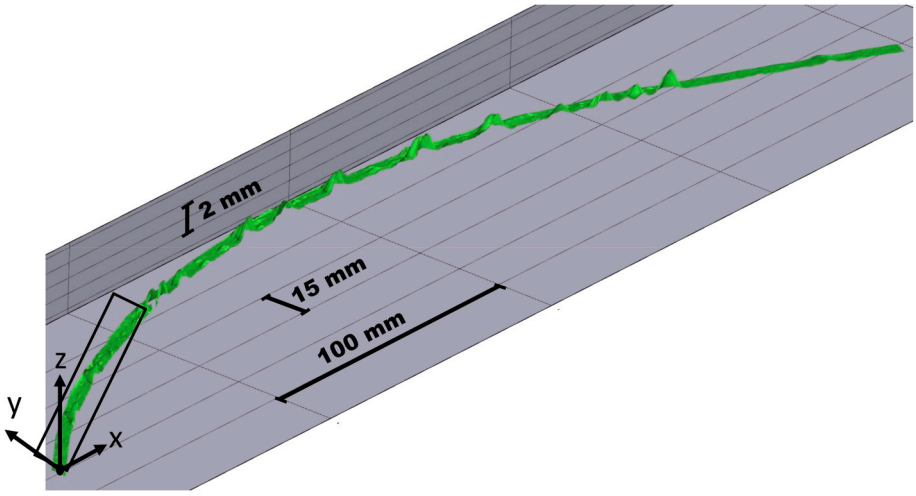

Fig. 11. Shape of the tow after placement along a circular path with ρ = 305 mm.

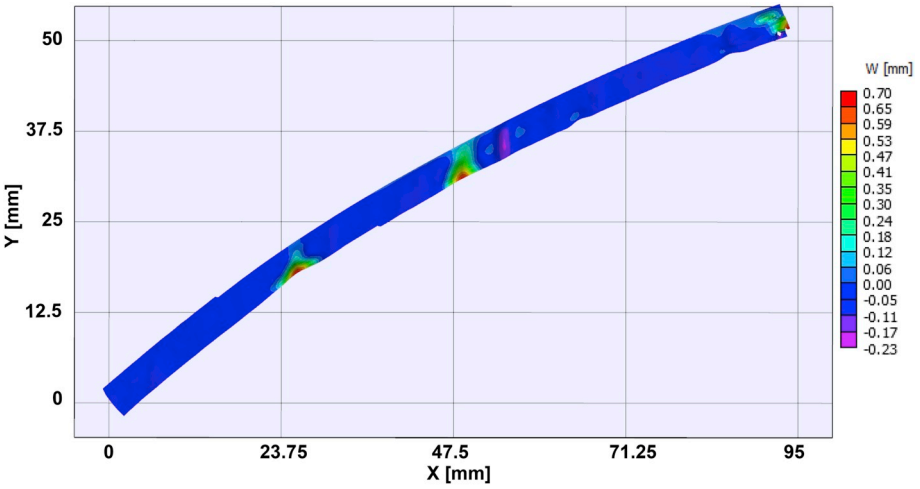

Fig. 12. Out-of-plane deformation map of the tow in the region highlighted by rectangular box in Fig. 11 for ρ = 305 mm.

wavelength, λ, and the width of the wrinkle as the wrinkle width, l_w, Table 3 presents the average value and variation of λ and l_w for ρ = 2540 mm, 1270 mm and 305 mm. Here, it is shown that as ρ decreases from 1270 mm to 305 mm, the mean value of wrinkle wavelength decreases by 1.5X. For wrinkles formed at substrate overlap locations, the amplitude increases by 2X and the wrinkle width increases by 1.16X. For wrinkles formed outside the substrate overlap regions, as ρ decreases from 1270 mm to 305 mm there is an order of magnitude increase in the amplitude and width of the wrinkles. With regard to λ, as shown in Table 3 there is relatively consistent wrinkle wavelength for ρ = 1270 mm, and much wider variability in wavelength for ρ = 305 mm. These experimental results indicate that high radii of curvature provide results that are nominally consistent with previous theoretical model predictions [12,13], whereas lower radii of curvature

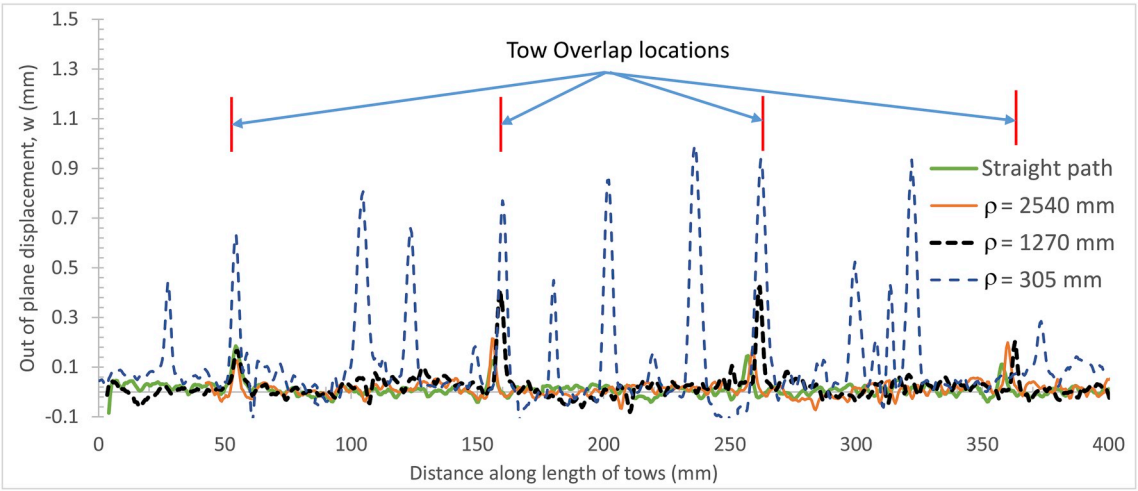

Fig. 13. Comparison of out of plane deformation along the length of tows placed with ρ = ∞, 2540 mm, 1270 mm and 305 mm. Plot corresponds to displacements along a line that is 1 mm above the bottom edge of the reference configuration in Fig. 1.

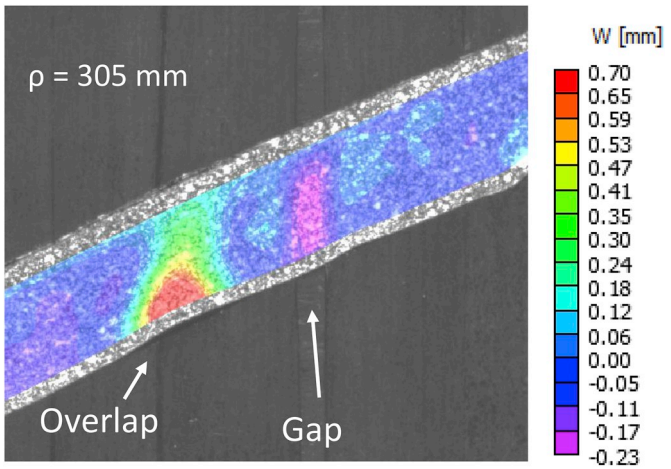

Fig. 14. Effect of gap and overlap in the substrate on the deformation for tow placed with ρ = 305 mm.

show much more variability in wrinkle wavelength. The low variability and consistency in the wrinkle wavelength for high values of ρ are nominally consistent with conditions that are used in typical plate/beam on elastic foundation models that are limited to relatively small deformations and displacements. The increased variability in λ for smaller ρ indicates that additional nonlinearities are present in the mechanics of wrinkle formation that are not included in these models. Variability in the wavelength of wrinkles is also reported in Ref. [18], where the authors placed 6.35 mm tows along curvilinear paths with ρ in the range of 558.8 –2032 mm with wrinkles observed for ρ = 558.8 mm and 635 mm.

3.3. Time and temperature effect on the wrinkled shape of tow: full-field displacement and deformations for ρ = 305 mm

In order to investigate viscoelastic effects of the tow, a separate experiment is carried out for a tow that is placed at ρ = 305 mm. The substrate imperfections due to overlap and gaps are minimized in this lay-up process by improving the substrate quality. This reduced variability in the wrinkle wavelength compared to the previous experiment (compare Figs. 13 and 16). Fig. 15 shows the out-of-plane displacement fields for a magnified region of the tow that has been steered with ρ = 305 mm at three specific stages. The in-plane coordinates shown in each figure correspond to the reference material directions for the tow prior to placement. Fig. 15a [12] shows the stage one conditions where the out of plane displacement data is obtained immediately after lay-up of the tow. Fig. 15b shows the out of plane displacement data obtained one hour after lay-up. Measurements in Fig. 15c are obtained just after re-heating of the tow occurred when the AFP heat source passed by close to the tow path. To simplify comparison of the data shown in Fig. 15, results for the complete length of the tow along a horizontal line located 1 mm above the lower tow edge on the compressive side of the tow are shown in Fig. 16.

4. Additional discussion of results

The out-of-plane wrinkle shapes for the AFP manufactured tow shows significant differences from the wrinkle shapes of tows when there is no adhesion [19]. When there is *no adhesion*, it was shown that wrinkling occurs on the compressive side of the tow and only a single wrinkle occurs along the entire length of the tow, when adhesion is present, multiple wrinkles are formed on the compressive side.

If the adhesion is of sufficient strength to prevent uplift on the tensile side of the tow, the relatively inextensible carbon fibers on the tensile side are sufficiently restrained to remain in plane. In this case, the fibers tend to slide transversely towards the neutral surface, reducing the distance between them while minimizing the axial strain in the fibers. The "macroscopic" transverse Lagrangian strain associated with the observed sliding of fibers is shown in Fig. 17 for ρ = 305 mm.

As noted in the previous section, the wrinkle shapes and wrinkle positions in tows with ρ = 305 mm during the AFP process are much more complex (see Figs. 13, 15 and 16) than the assumed shape used for analytical modeling in the published literature [12,13], with non-linearities such as the interaction of prepreg tow wrinkling deformation with highly nonlinear cohesive forces between the uncured tow and the laminate substrate contributing to the measured wrinkling response. As shown in the measurements in Fig. 13 and highlighted previously, existing surface defects on the substrate act as nucleation sites for local wrinkling of the tow, most likely due to the lack of adhesion between the substrate and the tow at such locations. For smaller ρ, the substrate-induced wrinkles are supplemented by additional wrinkling sites. When the tow is steered with ρ = 305 mm, eighteen local wrinkle locations are observed over a length of 400 mm of the tow, with an average wavelength of 21.30 mm and a standard deviation in the wavelength of

[12] Displacement data shown in Fig. 15a, b and c are between horizontal axis position of 165 mm and 240 mm. This region is a subset of the displacement data along the entire tow length that is shown in Fig. 16.

Table 3
Average wavelength, amplitude of wrinkles for different radii of curvature.

ρ (mm)	Number of wrinkles for length of 400 mm	Wavelength λ (mm)	Width l_w (mm)	Amplitude (mm)	Remarks
∞	4	100.10 ± 0.63	6.62 ± 0.97	0.136 ± 0.033	Wrinkle only at substrate overlap locations.
2540	4	101.14 ± 0.66	6.02 ± 1.61	0.172 ± 0.045	Wrinkle only at substrate overlap locations
1270	12	102.09 ± 0.61	7.80 ± 1.45	0.296 ± 0.145	Four wrinkles at substrate overlap locations.
		30.25 ± 8.89[c]	1.45 ± 0.75[a]	0.062 ± 0.022[a]	Eight small amplitude wrinkles at non-overlap substrate locations
305	18	106.57 ± 1.36	9.04 ± 2.87	0.644 ± 0.242	Four wrinkles at substrate overlap locations. Twelve wrinkles at non-
305	22[b]	21.30 ± 12.93[c]	8.03 ± 1.77[a]	0.488 ± 0.308[a]	overlap substrate locations.
		15.55 ± 7.14[b]	7.26 ± 2.32[b]	0.504 ± 0.324[b]	Twenty-two wrinkles observed at non-overlap substrate locations.[b]

[a] Wrinkles at non-overlap substrate locations.
[b] Tow lay-up on a substrate with reduced overlaps and gaps.
[c] Mean and standard deviation of wavelength calculated by considering all the wrinkles at substrate overlap and non-overlap locations.

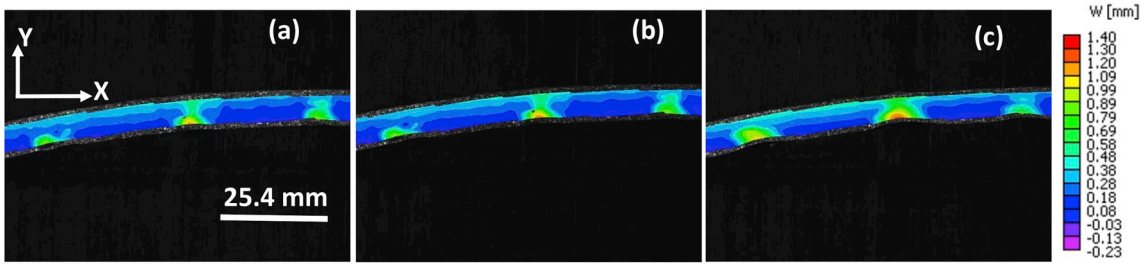

Fig. 15. Out-of-plane deformation map of a portion of the tow with ρ = 305 mm (a) immediately after placement (b) one hour after placement and (c) after applying heating to the tow. The portion of the tow is between 165 mm and 240 mm from the left end of the tow in the reference configuration.

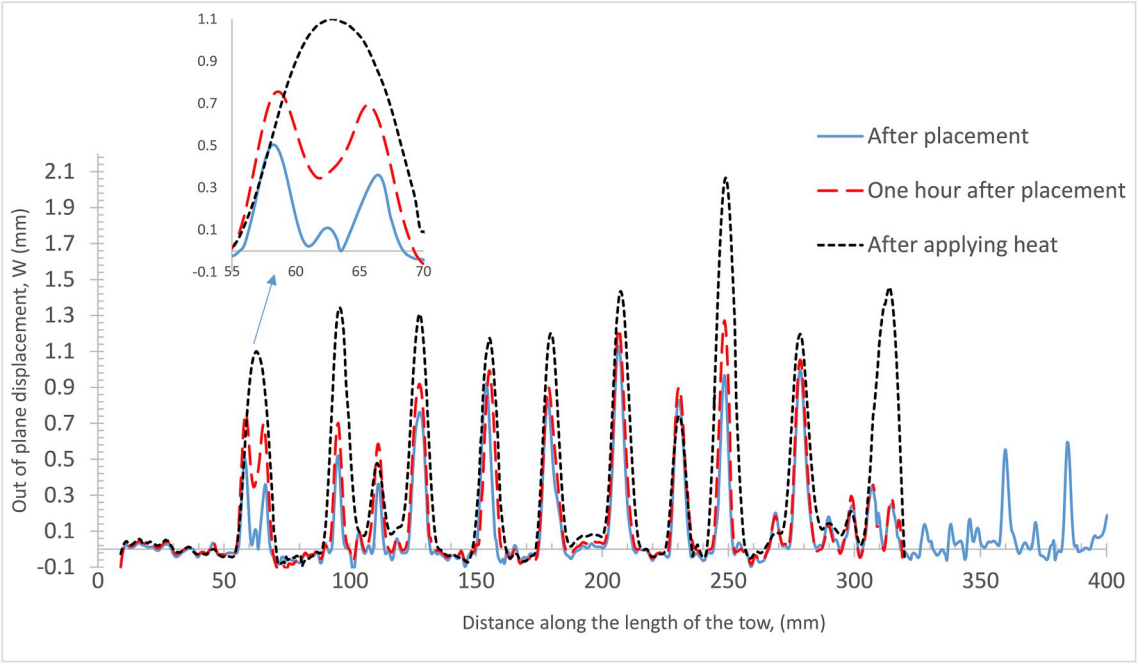

Fig. 16. Out-of-plane deformation along a line 1 mm above the bottom edge of the reference configuration for ρ = 305 mm. INSET: Magnified portion of the displacement plot showing merging of two wrinkles. Region beyond 320 mm separated from substrate just before one hour so no additional measurements available.

12.93 mm. The average wavelength observed is nominally consistent with results in Ref. [12]. Though quantitative data on the variability in the wavelength is not available in the published literature, photographs of the wrinkle pattern in Ref. [12] indicate a non-uniform spacing of the wrinkles. The presence of variability in the frequency of occurrence of wrinkles also is reported in Ref. [18].

Results from a second lay-up experiment with reduced substrate overlaps and gaps (Fig. 16) show that the number of wrinkles increases (wavelength decreases) and variability in the wrinkle spacing decreases compared to the first lay-up experiment on a substrate with significant overlaps and gaps (Fig. 13). In addition, the average amplitude and width of the wrinkles decreases in the second lay-up experiment. A plausible reason for the lower number of wrinkles with increased amplitude and width at substrate overlap locations in the first experiment is that the measured larger l_w values results in additional energy release in these regions and less energy available to initiate new wrinkles.

As shown in Fig. 16, during the first hour after placement, tow wrinkle amplitude increases as the temperature of the tow reaches ambient levels in the laboratory. After the tow is re-heated without additional mechanical loading, there can be marked changes in the out-of-plane wrinkle shape for

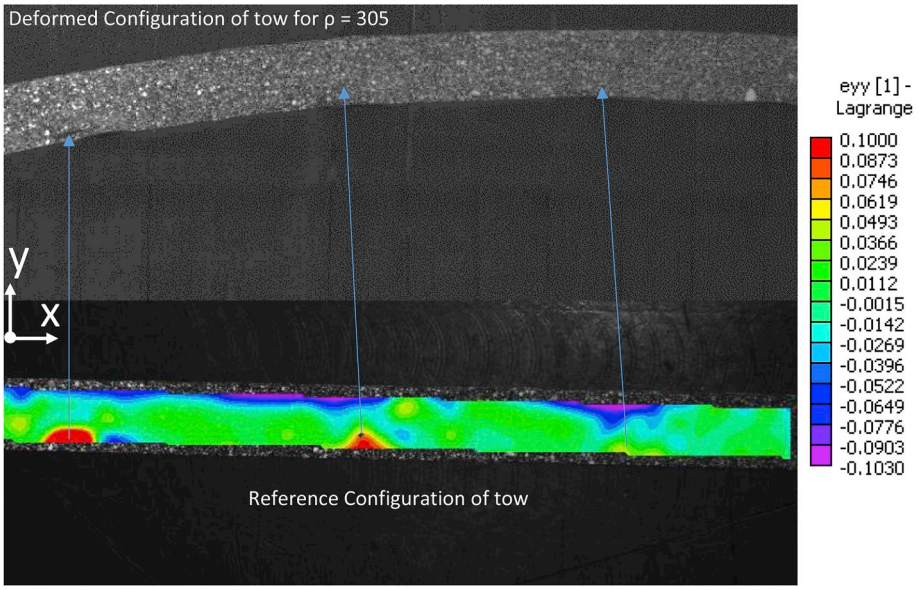

Fig. 17. Transverse Lagrangian strain map on the surface of the tow immediately after placement with ρ = 305 mm for the region shown in Fig. 15. The arrows represent mapping of the material points from the reference to deformed configuration.

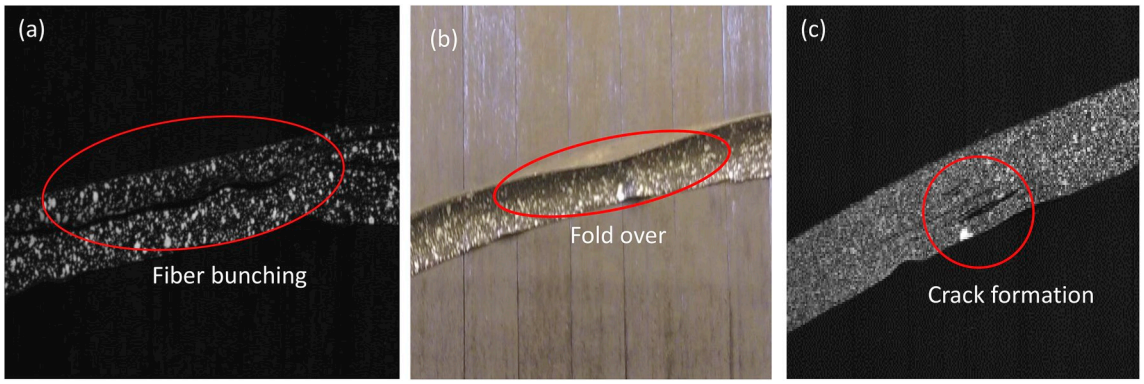

Fig. 18. Commonly observed defect other than wrinkling in tows steered along curvilinear paths such as (a) fiber bunching, (b) fold over and (c) matrix failure.

the tow. For example, as shown in Fig. 16, two of the adjacent wrinkles merge into one large wrinkle. These experiments show that time and temperature-dependent properties of the binder material can influence the amplitude and coalescence of adjacent wrinkles, especially when fibers are steered at smaller radii of curvatures. Though the amplitude of the wrinkles increased with time, no new wrinkles are observed to form during the first one hour. In this regard, careful observation of the layup process showed that the wrinkles initiate immediately after the roller pressure is released. Hence, the experimental evidence strongly suggests that the initiation "toughness" for wrinkle formation will not be a function of time.

Though the primary focus of this work is related to quantifying wrinkling as a function of radius of curvature during AFP, additional commonly observed defects during tow placement include (a) bunching of fibers, (b) folding over of tows during placement and (c) crack formation/matrix failure; Fig. 18 shows photographs of these defects,[13] with Fig. 18a showing a severe case of fiber bunching combined with matrix failure. In our definition of fiber bunching, the results in Fig. 17 for the transverse strain are an indicator that "fiber bunching" is occurring in our experiments. In addition, as shown in Fig. 18b and c, the investigators also observed both tow fold-over and fiber-matrix cracking during these studies. The defects shown in Fig. 18a and b are mainly observed in regions of poor adhesion of the tow with the substrate. The separation and crack formation shown in Fig. 18c are a function of the relatively weak uncured tow matrix and the presence of modest transverse tensile strains on the side closer to the inner radius. Another form of defect, in-plane wrinkling, is reported in Ref. [18]. However, for the selected radii of curvature, tow materials and process parameters, our experiments do not show any indication of in-plane wrinkling based on the measured strain or displacement data. One of the reasons for occurrence of in-plane wrinkles in Ref. [18] could be due to the low adhesion of the tow with the aluminum tool, whereas in our layup experiments, the tows were placed on a substrate of the same material. The absence of indications of in-plane wrinkling suggests that this could be caused by higher energy being required to overcome the bonding stresses for inducing in-plane wrinkling (when compared to conditions for out of plane wrinkling and other forms of deformation seen in our experiments).

5. Summary

For the first time, an experimental investigation using StereoDIC to obtain in-situ measurements is presented quantifying out-of-plane wrinkle formation and in-plane deformations occurring in prepreg slit tape during automated fiber placement (AFP) and adherence of tows to a composite laminate substrate. The methodology is employed to obtain deformation of 6.35 mm wide thermoset prepreg tow after lay-up using

[13] Since these defects result in either obscuring or damage of the speckle images beyond recognition, correlation of the deformed and reference speckle images is difficult.

AFP process to understand the effect of steering radius of curvature, ρ, time and temperature on wrinkle formation. The tow lay-up process is performed for a range of ρ using an industrial-scale AFP machine (Horizontal Lynx® AFP from Ingersoll Machine Tools), with full field three-dimensional tow shape and surface deformation measurements performed (a) immediately after lay-up of the tow, (b) one hour after lay-up and (c) shortly after applying heating to the already placed tow by traversing the AFP head with infrared heat source close to the tow path. Results from our experimental studies give the following observations.

- Tow wrinkling is observed in all tows at each location where the underlying laminate substrate showed surface defects such as tow overlaps and gaps.
- For straight paths and for a circular path with radius of curvature, R = 2540 mm, no additional out-of-plane wrinkles are observed away from the tow overlap locations.
- For circular paths with R = 1270 mm and 305 mm, additional wrinkles are observed with mean wavelengths of 30.25 mm and 21.3 mm with standard deviations of 8.89 mm and 12.93 mm, respectively. The amplitudes of the additional out-of-plane wrinkles for R = 1270 mm are on the order of the thickness of the tow. However, for R = 305 mm, the amplitudes of the wrinkles are an order of magnitude larger.
- For the shortest radius of curvature (R = 305 mm), the lay-up process is performed (a) on a substrate having defects (overlaps) at intervals of 100 mm and (b) on a substrate with no defects. For AFP lay-up trial (a), the wrinkle wavelength showed larger variability; mean value of 21.30 mm with a standard deviation of 12.93 mm. For trial (b) that had no surface defects, the mean wavelength is 15.55 mm with a standard deviation of 7.14 mm. The variability in the wavelength of wrinkles cannot be predicted by existing wrinkle models [12,13] that assumes a uniform spacing.
- During the first hour of lay-up, tow wrinkle amplitude increases to almost twice the amplitude of the wrinkle immediately after placement, apparently due to viscoelastic effects in the prepreg tack. However, the wrinkle mode shapes remain the same.
- After applying heating to the steered tow, wrinkles which are close to each other tend to merge into one large wrinkle, apparently due to considerable loss in stiffness of the cohesive layer between the tow and substrate.

Currently, a non-linear finite element-based model incorporating a mixed mode cohesive traction-separation relationship for modeling the tow-substrate interaction is ongoing. Since the simulations require the mixed mode traction-separation relationship for the bonded tows, the authors are also developing a novel specimen to perform mixed Mode I/II experiments with the tows. Results from these ongoing studies will be the subject of future publications.

Acknowledgements

Funding provided by Boeing Research Contract SSOWBRTW0915000 and associated matching funds provided by University of South Carolina Vice President for Finance Edward Walton via 15540 E250 is deeply appreciated. All materials and access to the Lynx® AFP facility provided by the McNair Aerospace Center, University of South Carolina is gratefully acknowledged. The technical support and assistance of the McNair technical staff, particularly Mr. Burton Rhodes, Jr., during operation of the AFP is also greatly appreciated. Finally, the support of Ms. Eileen Miller, Boeing Research and Technology in Charleston, SC, is gratefully acknowledged.

References

[1] Nayak NV. Composite materials in aerospace applications. Int J Sci Res Publ 2014;4:2250–3153.
[2] Lopes CS, Gürdal Z, Camanho PP. Variable-stiffness composite panels: buckling and first-ply failure improvements over straight-fibre laminates. Comput Struct 2008;86:897–907. https://doi.org/10.1016/j.compstruc.2007.04.016.
[3] Gürdal Z, Tatting BF, Wu CK. Variable stiffness composite panels: effects of stiffness variation on the in-plane and buckling response. Compos Part A Appl Sci Manuf 2008;39:911–22. https://doi.org/10.1016/j.compositesa.2007.11.015.
[4] Gürdal Z, Olmedo R. In-plane response of laminates with spatially varying fiber orientations - variable stiffness concept. AIAA J 1993;31:751–8. https://doi.org/10.2514/3.11613.
[5] Chen X, Wu Z, Nie G, Weaver P. Buckling analysis of variable angle tow composite plates with a through-the-width or an embedded rectangular delamination. Int J Solid Struct 2018;138:166–80. https://doi.org/10.1016/J.IJSOLSTR.2018.01.010.
[6] Wu Z, Raju G, Weaver PM. Optimization of postbuckling behaviour of variable thickness composite panels with variable angle tows: towards “Buckle-Free” design concept. Int J Solid Struct 2018;132(133):66–79. https://doi.org/10.1016/J.IJSOLSTR.2017.08.037.
[7] Crosky A, Grant C, Kelly D, Legrand X, Pearce G. 4 – fibre placement processes for composites manufacture. Adv Compos Manuf Process Des 2015:79–92. https://doi.org/10.1016/B978-1-78242-307-2.00004-X.
[8] Long AC, Clifford MJ. Composite forming mechanisms and materials characterisation. Compos Form Technol 2007:1–21. https://doi.org/10.1533/9781845692537.1.
[9] Abdi F, Gürdal Z, Huang D. Certification modeling of composites fuselage, considering effect of defects from fiber placement manufacturing processes. 55th AIAA Aerosp. sci. Meet Reston, Virginia: American Institute of Aeronautics and Astronautics; 2017. https://doi.org/10.2514/6.2017-0691.
[10] Khani A, Abdalla MM, Gürdal Z. Optimum tailoring of fibre-steered longitudinally stiffened cylinders. Compos Struct 2015;122:343–51. https://doi.org/10.1016/j.compstruct.2014.11.071.
[11] Oromiehie E, Gangadhara Prusty B, Compston P, Rajan G. *In-situ* simultaneous measurement of strain and temperature in automated fiber placement (AFP) using optical fiber Bragg grating (FBG) sensors. Adv Manuf Polym Compos Sci 2017;3:52–61. https://doi.org/10.1080/20550340.2017.1317447.
[12] Matveev MY, Schubel PJ, Long AC, Jones IA. Understanding the buckling behaviour of steered tows in automated dry fibre placement (ADFP). Compos Part A Appl Sci Manuf 2016;90:451–6. https://doi.org/10.1016/j.compositesa.2016.08.014.
[13] Beakou A, Cano M, Le Cam J-B, Verney V. Modelling slit tape buckling during automated prepreg manufacturing: a local approach. Compos Struct 2011;93:2628–35. https://doi.org/10.1016/j.compstruct.2011.04.030.
[14] Boisse P, Hamila N, Madeo A. Modelling the development of defects during composite reinforcements and prepreg forming. Philos Trans R Soc A Math Phys Eng Sci 2016;374:20150269. https://doi.org/10.1098/rsta.2015.0269.
[15] Guzman-Maldonado E, Hamila N, Boisse P, Bikard J. Thermomechanical analysis, modelling and simulation of the forming of pre-impregnated thermoplastics composites. Compos Part A Appl Sci Manuf 2015;78:211–22. https://doi.org/10.1016/J.COMPOSITESA.2015.08.017.
[16] Boisse P, Colmars J, Hamila N, Naouar N, Steer Q. Bending and wrinkling of composite fiber preforms and prepregs. A review and new developments in the draping simulations. Compos Part B Eng 2018;141:234–49. https://doi.org/10.1016/J.COMPOSITESB.2017.12.061.
[17] Sherwood J, Fetfatsidis K, Winchester D, Jauffrès D, Avitabile P, Chen J. Using modal analysis to investigate the validity of finite element models for simulating the thermostamping of woven-fabric reinforced composites. Int J Mater Form 2010;3:687–90. https://doi.org/10.1007/s12289-010-0863-4.
[18] Nima B, Mehdi H. An experimental and simulative study on the defects appeared during tow steering in automated fiber placement. Compos Part A Appl Sci Manuf 2018;113:122–31. https://doi.org/10.1016/j.compositesa.2018.07.031.
[19] Rajan S, Sutton MA, Wehbe R, Tatting B, Gürdal Z. Measured surface deformation and strains in thin thermoplastic prepreg tapes steered along curved paths without adhesion using StereoDIC (in review).
[20] Sutton MA, McNeill SR, Helm JD, Chao YJ. Advances in two-dimensional and three-dimensional computer vision. Photomechanics Berlin, Heidelberg: Springer Berlin Heidelberg; 2000. p. 323–72. https://doi.org/10.1007/3-540-48800-6_10.
[21] Helm JD, McNeill SR, Sutton MA. Improved three-dimensional image correlation for surface displacement measurement. Soc Photo-Optical Instrum Eng 1996;35:1911–20. https://doi.org/10.1117/1.600624.
[22] Sutton MA. Computer vision-based, noncontacting deformation measurements in mechanics: a generational transformation. Appl Mech Rev 2013;65:050000https://doi.org/10.1115/1.4024984.
[23] Luo PF, Chao YJ, Sutton MA. Application of stereo vision to three-dimensional deformation analyses in fracture experiments. Opt Eng 1994;33:3.
[24] Luo PF, Chao YJ, Sutton MA, Peters WH. Accurate measurement of three-dimensional deformations in deformable and rigid bodies using computer vision. Exp Mech 1993;33:123–32. https://doi.org/10.1007/BF02322488.
[25] Wang W, Mottershead JE, Ihle A, Siebert T, Reinhard Schubach H. Finite element model updating from full-field vibration measurement using digital image correlation. J Sound Vib 2011;330:1599–620. https://doi.org/10.1016/j.jsv.2010.10.036.
[26] Correlated Solutions – VIC-3D™ n.d. http://correlatedsolutions.com/vic-3d/ (Accessed June 26, 2017).
[27] Sutton MA, Orteu J-J, Schreier H. Image correlation for shape, motion and deformation measurements. Boston, MA: Springer US; 2009. https://doi.org/10.1007/978-0-387-78747-3.
[28] Sutton MA, Matta F, Rizos D, Ghorbani R, Rajan S, Mollenhauer DH, et al. Recent progress in digital image correlation: background and developments since the 2013 W M Murray lecture. Exp Mech 2017;57:1–30. https://doi.org/10.1007/s11340-016-0233-3.